

Electrical characterization of benzenedithiolate molecular electronic devices with graphene electrodes on rigid and flexible substrates

Yeonsik Jang¹, Hyunhak Jeong¹, Dongku Kim¹, Wang-Taek Hwang¹, Jun-Woo Kim¹, Inho Jeong², Hyunwook Song², Jiyoung Yoon¹, Gyu-Chul Yi^{1,3}, Heejun Jeong³ and Takhee Lee¹

¹ Department of Physics and Astronomy, and Institute of Applied Physics, Seoul National University, Seoul 08826, Korea

² Department of Applied Physics, Kyung Hee University, Yongin-si, Gyeonggi-do 17104, Korea

³ Department of Applied Physics, Hanyang University, Ansan, Gyeonggi-do 15588, Korea

E-mail: hjeong@hanyang.ac.kr and tlee@snu.ac.kr

Received 19 December 2015, revised 24 January 2016

Accepted for publication 1 February 2016

Published 23 February 2016



CrossMark

Abstract

We investigated the electrical characteristics of molecular electronic devices consisting of benzenedithiolate self-assembled monolayers and a graphene electrode. We used the multilayer graphene electrode as a protective interlayer to prevent filamentary path formation during the evaporation of the top electrode in the vertical metal–molecule–metal junction structure. The devices were fabricated both on a rigid SiO₂/Si substrate and on a flexible poly(ethylene terephthalate) substrate. Using these devices, we investigated the basic charge transport characteristics of benzenedithiolate molecular junctions in length- and temperature-dependent analyses. Additionally, the reliability of the electrical characteristics of the flexible benzenedithiolate molecular devices was investigated under various mechanical bending conditions, such as different bending radii, repeated bending cycles, and a retention test under bending. We also observed the inelastic electron tunneling spectra of our fabricated graphene–electrode molecular devices. Based on the results, we verified that benzenedithiolate molecules participate in charge transport, serving as an active tunneling barrier in solid-state graphene–electrode molecular junctions.

Keywords: molecular electronics, benzenedithiolates, multilayer graphene (MLG), flexible electronics, inelastic electron tunneling spectroscopy (IETS)

(Some figures may appear in colour only in the online journal)

1. Introduction

Molecular electronics, in which single molecules or molecular monolayers are used as active components of electronic devices, has been widely studied as the ultimate miniaturization of electronic devices [1–10]. Various attempts have been made to produce molecular junctions for the purpose of investigating the characteristics of charge transport in the molecular regime, using approaches such as mechanically

controllable break junctions (MCBJs), electromigrated nano-gap fabrication, scanning probe microscopy, the fabrication of eutectic gallium–indium junctions, and various solid-state device fabrication methods [2, 9, 11–17]. In particular, vertical-type solid-state devices based on an evaporated metal–molecule–metal junction structure have received significant attention as a general test-bed platform for investigating the charge transport characteristics of molecular junctions. However, the direct metal evaporation process used to form

the top electrode can easily create electrical shorts via the formation of filamentary paths through the molecules, which results in junctions that are unsuitable for characterization [18–24]. To solve this problem, various approaches have been proposed, for example, introducing an interlayer between the top metal electrode and molecular layers conducting polymer poly(3,4-ethylenedioxythiophene) polystyrene sulfonate (PEDOT:PSS), multilayer graphene (MLG), or reduced graphene oxide [25–34]. In addition, novel fabrication techniques in which the top electrode can be produced without causing damage to the molecular layer, such as direct transfer methods, have been proposed [35, 36]. The ultimate aim of these various approaches is to improve the reliability of molecular electronic devices. Among these methods, MLG–interlayer-based molecular junctions in particular offer various advantages by virtue of their graphene electrodes. Graphene is a two-dimensional sheet of carbon atoms with excellent electronic properties [37, 38]. It can be synthesized as large-area, flexible, and conductive films that are suitable for use as electrodes [39, 40]. Using such graphene films as interlayer electrodes in molecular junctions, a previous study demonstrated a high device yield and stability over a long period, accompanied by the capability of mass production, nontoxicity, and low contact resistance comparable to that of pure metal–molecule–metal junctions [29]. However, to date, only one kind of molecule (i.e., alkanethiolate) has been studied as a test-bed molecule for this type of molecular junction. In addition, the fabrication of graphene–interlayer molecular junctions on flexible substrates has not yet been demonstrated. It has only been demonstrated that molecular devices with a conducting polymer (PEDOT:PSS) interlayer can be fabricated using various kinds of molecules (alkanethiolates, diodes, and photoswitching molecules) on flexible substrates [26–28, 31, 34]. Furthermore, the inelastic electron tunneling spectroscopy (IETS) characteristics of graphene–interlayer molecular junctions has not yet been verified. Therefore, extending our understanding of graphene–interlayer molecular electronic devices is a great necessity.

In this study, we report the electrical characteristics of molecular electronic devices fabricated from benzenedithiolate self-assembled monolayers (SAMs), both on a rigid SiO₂/Si substrate and on a flexible poly(ethylene terephthalate) (PET) substrate. We used an MLG electrode as a protective interlayer to prevent electrical shorts in the vertical molecular junction structure. We investigated the fundamental charge transport characteristics of the benzenedithiolate molecular junctions. In particular, the reliability of the electrical characteristics of the flexible molecular devices was studied under various mechanical bending conditions. IETS of the graphene–interlayer benzenedithiolate molecular devices were also characterized.

2. Experimental details

Figure 1(a) shows a schematic illustration of the device fabrication process for our graphene–interlayer molecular

junctions. We followed the same junction fabrication process that we have previously reported [19, 28, 29, 35]. In brief, the bottom electrodes (30 nm Au/5 nm Ti) were first patterned via a shadow mask using an electron beam evaporator operating at a rate of 0.2 Å s⁻¹ on a p-type (100) SiO₂/Si (300 nm) or a flexible PET substrate. Then, optical lithography was used to create 2 μm radius holes through walls of photoresist (AZ5214E from AZ Electronic Materials). Each sample was immersed for 3 h in a 5 mM molecular solution diluted with ethanol in a N₂-filled glove box, causing SAMs to form on the exposed Au surfaces. For this study, we chose three different benzenedithiolate molecules: benzene-1,4-dithiol (BDT), biphenyl-4,4'-dithiol (BPDT), and p-terphenyl-4,4''-dithiol (TPDT), as shown in figure 1(c). After the SAM deposition, an MLG film was transferred to cover the surface of each sample using the direct metal transfer method, as we have previously reported [35]. To produce the MLG interlayer, an MLG film was first grown in a chemical vapor deposition chamber on a Ni (300 nm)/Ti (10 nm)/Si substrate (under a gas flow of 15 sccm CH₄ and 20 sccm Ar/H₂ at 20 Torr for 10 min at 900 °C). After growth was complete, a layer of poly(methylmethacrylate) (PMMA, 950PMMA A5 from MicroChem Corp.) was spin coated onto the film as a dummy layer, and support tape was attached to the PMMA. Then, the Ni of the substrate was etched using an iron(III) chloride (FeCl₃) aqueous solution. The MLG film was then placed onto the molecular layer to make contact through the van der Waals interaction. Afterward, a few drops of isopropyl alcohol (IPA) were applied to the molecular layer to form a fine contact via the surface tension of the IPA solution during its vaporization [41]. Then, the sample was dried for ~12 h, and the PMMA was removed with acetone. The top electrode was deposited in the same way as the bottom electrode (15 nm thick Au), using the same patterned shadow mask, with the evaporator operating at a rate of 0.1 Å s⁻¹. Finally, the remaining MLG film was removed by means of an oxygen plasma treatment under 10 sccm of O₂ gas at 50 W of forward power to prevent the formation of any direct pathway through the top and bottom electrodes. Electrical measurements were performed using a semiconductor parameter analyzer (Keithley 4200 SCS) and a probe station system (JANIS Model ST-500). Figure 1(b) presents optical, scanning electron microscopy (SEM), and cross-sectional transmission electron microscopy (TEM) images of our molecular devices fabricated on the rigid substrate. More detailed device fabrication schematics and the properties of the MLG film are provided in the supplementary information.

IETS measurements were performed at 4.2 K using a custom-made cryogenic vacuum chamber in which BDT molecular devices were mounted inside a liquid He dewar. Each device was placed on a 16-pin IC chip carrier socket and then electrically shielded inside the vacuum chamber. The detailed circuit diagram of the IETS setup is provided in figure 4(b). The current was measured using a digital multimeter (Agilent 34410) with a 16-bit digital-to-analog converter as a DC source and a low-noise current amplifier (Ithaco 1211). The first (dI/dV) and second (d^2I/dV^2) derivatives of the current with respect to the voltage were

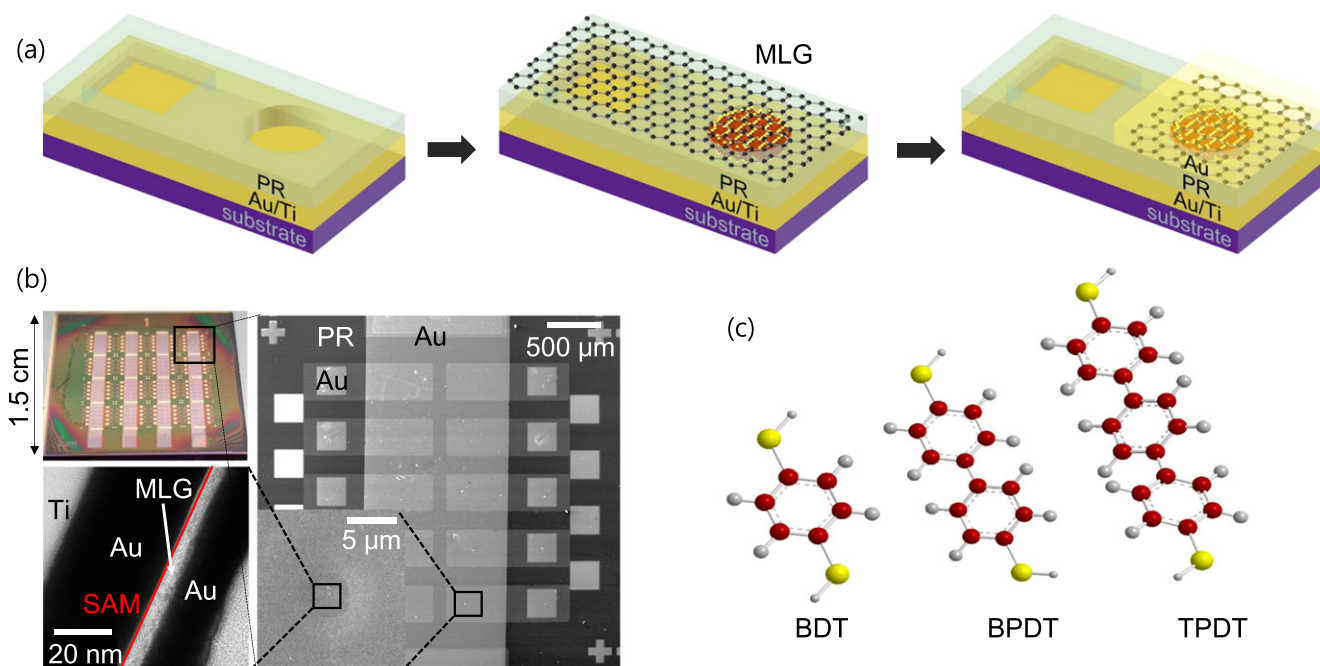


Figure 1. (a) Schematic illustration of the device fabrication process for the graphene–interlayer–electrode molecular junctions. Left: bottom electrode deposition and photoresist wall formation. Middle: SAM deposition and MLG transfer. Right: top electrode deposition and molecular device completion. (b) Optical, SEM, and TEM images of the molecular devices. (c) The three types of molecules with their chemical structures: BDT, BPDT, and TPDT.

measured following the standard AC modulation technique using a lock-in amplifier (LIA, Stanford Research Systems SR830). The root-mean-square (rms) AC modulation bias was 5 mV at a frequency of 503 Hz. The reference phase was -90° when the second harmonic was measured for d^2I/dV^2 (there was no phase shift for the first harmonic). Finally, the DC voltage was swept from 0 to 0.3 V.

3. Results and discussion

Although alkanethiolates are a common choice for molecular junction test-beds, benzene-based conjugate molecules are also important because their conjugate electronic structure can induce interesting electrical behaviors with various advantages [42–44]. We chose three types of benzenedithiolates because they are the simplest and most widely studied conjugate molecules in the field of molecular electronics and also one of the most promising families of prototype molecules for studying the fundamentals of charge transport. Choosing benzenedithiolate molecules allowed us to compare the data measured from our fabricated MLG–interlayer molecular junctions with those from benzenedithiolate molecular junctions fabricated using other known methods. Various studies have indicated that the primary mechanism of charge transport through benzenedithiolate is non-resonant tunneling (when the applied voltage is not too high), in which the current density exhibits an exponential dependence on the molecular length, as in the case of alkanethiolates [45–48]. However, because conjugate molecules have far smaller gaps between the highest occupied molecular orbital and the lowest

unoccupied molecular orbital than do saturated molecules such as alkanethiolates, higher conductance is expected. By replacing BDT with BPDT and TPDT (thereby increasing the number of phenyl rings), we could measure the decay coefficient (β) per phenyl ring and compare this β value with previously reported values [45–49]. Figure 2(a) shows the statistically derived current density–voltage (J – V) characteristics on a logarithmic scale for all working BDT, BPDT, and TPDT molecular devices with graphene electrodes on the rigid SiO_2/Si substrate. Comparison of J – V characteristics between Au/BDT/Au, Au/MLG/BDT/Au, and Au/PEDOT:PSS/BDT/Au junctions was given in the supplementary information. We fabricated a sufficient number of devices to conduct a statistical analysis for each type of molecular junction, and we identified the operating devices by fitting the histograms based on a Gaussian distribution function. The range of operation for the devices was determined to extend from $\mu - \sigma$ to $\mu + \sigma$ where μ is the Gaussian average of the current density (in units of A cm^{-2}) at 1 V and σ is the Gaussian standard deviation. The error bars marked at ± 1 V represent the standard deviations of the operating devices. From the operating devices, the log-averaged current densities (J) at 1 V for BDT, BPDT, and TPDT were found to be 2.90 A cm^{-2} , 2.39 A cm^{-2} , and 1.62 A cm^{-2} , respectively. These results indicate that the current density decreases with an increasing number of phenyl rings. Note that the difference per ring is smaller than that observed in the case of alkanethiolate molecular junctions because benzenedithiolate molecules form a smaller tunneling barrier than do alkanethiolates, i.e., benzenedithiolate molecules exhibit a smaller tunneling decay coefficient (β). Figure 2(b) presents a semi-

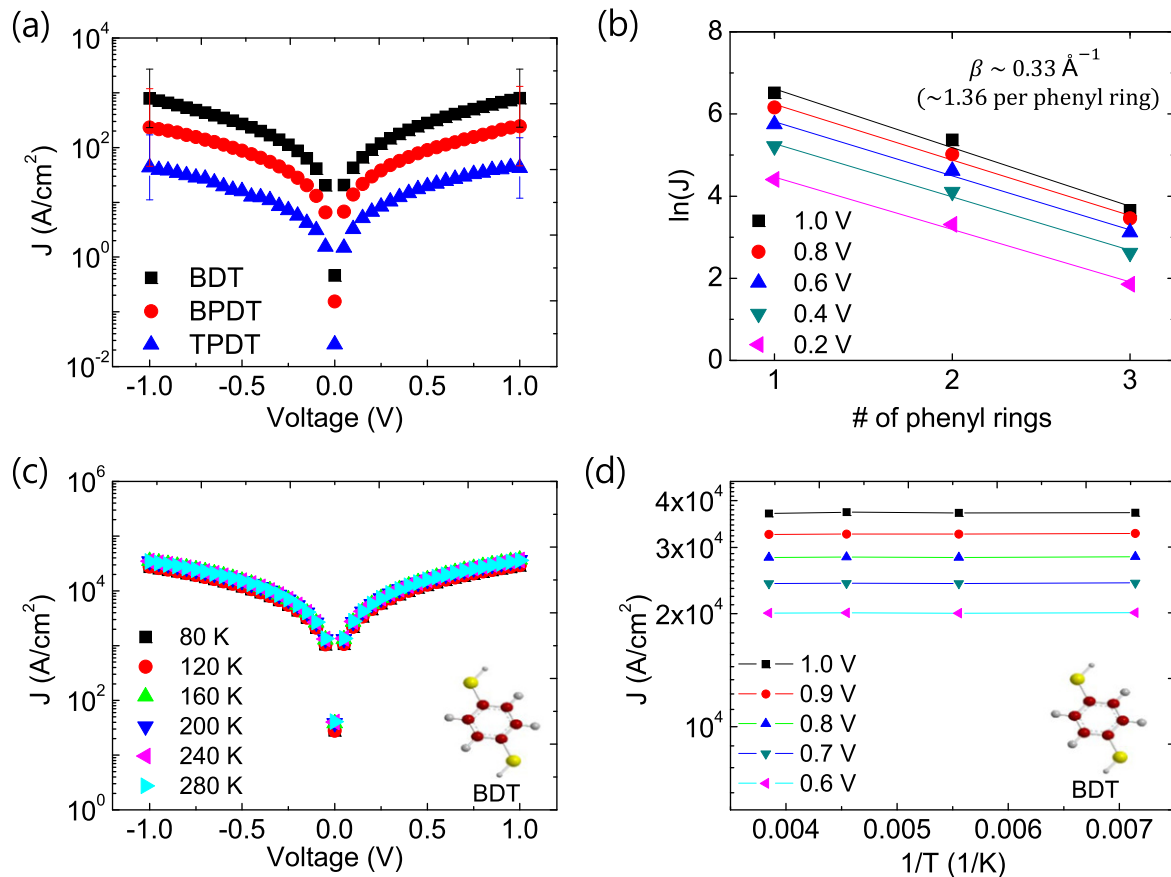


Figure 2. (a) Statistically derived J - V characteristics of all working BDT, BPDT, and TPDT molecular devices with graphene electrodes. (b) A semi-log plot of the J values at different biases versus the numbers of phenyl rings in the BDT, BPDT, and TPDT molecular devices. (c) Semi-log plot of the current densities measured at different biases from 0.2 to 1 V as a function of the molecular length. This graph shows an exponential decrease in the current density as the molecular length increases. (d) J - V - T measurements of a BDT molecular device. The temperature was varied from 80 to 280 K in increments of 40 K. (e) Arrhenius plot of the J - V - T measurements of the BDT device, presented to verify the type of charge transport occurring in the device.

log plot of the J values at different biases, from 0.2 to 1 V, versus the numbers of phenyl rings in the molecules of the BDT, BPDT, and TPDT devices. This graph shows an exponential decrease in the current density as the molecular length increases. Based on the non-resonant tunneling model ($J = J_0 e^{-\beta d}$, where β is the decay coefficient and d is the molecular length), we could determine β by performing a linear fit for each bias. The average β value was found to be $0.33 \pm 0.02 \text{ \AA}^{-1}$ (1.36 ± 0.06 per phenyl ring), in good agreement with previously reported values [45–48]. To determine the characteristics of the tunneling transport through our molecular junctions, we performed a temperature-varying current density-voltage (J - V - T) analysis to identify the temperature dependence of the J - V characteristics. Figure 2(c) depicts the J - V - T measurements of the BDT molecular devices. The temperature was varied from 80 to 280 K in increments of 40 K. Figure 2(d), which represents an alternate means of plotting the dataset presented in figure 2(c), shows the Arrhenius plot (J versus $1/T$) to verify the type of charge transport occurring in the device. This graph shows the temperature-independent characteristics of the current density, which imply that the primary mechanism of charge transport in our molecular junctions is indeed non-

resonant tunneling; this is consistent with the results of previous studies [47, 48].

We also fabricated the same BDT molecular devices with MLG electrodes on a flexible PET substrate. PET is attractive for use as a substrate for molecular junctions because it offers various advantages such as outstanding durability, thermal stability, and weatherproofness [50, 51]. Moreover, PET is insoluble by organic solvents such as ethanol and acetone. Because our device fabrication process entails several steps of solution processing (SAM deposition in an ethanol solution and PMMA removal in acetone), a PET substrate is a suitable choice for the fabrication of our molecular devices. Figure 3(a) shows the J - V curve for the BDT molecular devices on the PET flexible substrate under flat conditions (bending radius = ∞). This graph shows that the order of the current density is the same as that for the devices fabricated on the rigid substrate. The reliability of the electrical characteristics of the flexible molecular devices was also examined under various bending conditions. Figure 3(b) presents the current densities measured at 0.8 V under different bending configurations (bending radii of ∞ , 10 mm, and 5 mm). The current density remained nearly constant regardless of the bending radius. This result demonstrates that

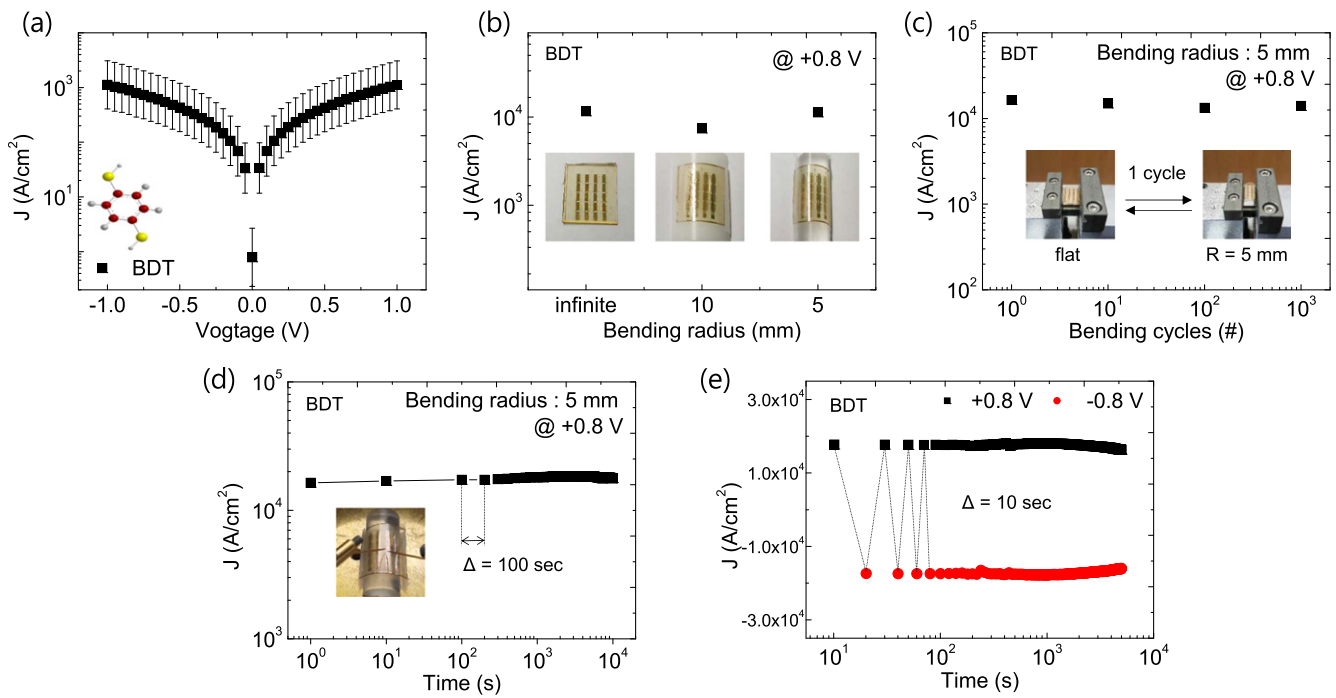


Figure 3. (a) J - V curve for the BDT molecular devices on the flexible substrate under flat conditions (bending radius = ∞). (b) Current densities measured at 0.8 V in different bending configurations (bending radii of ∞ , 10 mm, and 5 mm). (c) J - V characteristics measured throughout 10^3 bending cycles of repeated 5 mm radius bending using a bending machine. (d) Retention characteristics of a molecular device with a 5 mm bending radius. A voltage of 0.8 V was applied in intervals of a duration that was increased in increments of 100 s up to 10^4 s. (e) Retention characteristics with voltage switching between +0.8 and -0.8 V at intervals of 10 s, where the current persisted up to 5000 s.

the electrical characteristics of our molecular devices do not degrade under mechanical distortion. Figure 3(c) shows the J - V characteristics measured throughout 10^3 bending cycles of repeated 5 mm radius bending using a bending machine (see the inset of figure 3(c)). This result confirms the endurance of our devices under continuous, repeated mechanical stress. We also performed a retention test with a 5 mm bending radius, as shown in figure 3(d). A voltage of 0.8 V was applied for intervals of a duration that was increased in increments of 100 s. Under these conditions, the currents were maintained for up to 10^4 s. Figure 3(e) shows the result of a similar measurement conducted with voltage switching between +0.8 and -0.8 V at intervals of increasing duration in increments of 10 s, in which the currents were again well maintained for up to 5000 s. In addition to bending tests, we also examined the stability of flexible devices by analyzing bending strain ε of devices for each bending radius R , which is given in the supplementary information. Based on these results, we can confirm that the electrical characteristics of our molecular devices with MLG electrodes are well preserved regardless of mechanical stress.

In addition to fundamental current-voltage characterization and temperature-varying measurements, various techniques are available for investigating the charge transport characteristics of molecular junctions, including transition voltage spectroscopy, noise spectroscopy, thermoelectric measurements, surface-enhanced Raman spectroscopy, and IETS [52–56]. IETS in particular has been proposed as a powerful tool for the detection of unique vibration modes of molecules in a tunneling junction. Several studies have been

performed concerning IETS measurements of alkanethiolate SAMs in nanopore structures, single alkanethiolate or BDT molecules in MCBJs, and electromigrated nanogap junctions, as well as the use of scanning tunnel microscope techniques [48, 57–60]. Recently, we reported the results of IETS measurements of pure metal-molecule-metal solid-state junctions fabricated using a direct transfer method [36]. However, the IETS characteristics of graphene-interlayer molecular devices have not yet been verified. Thus, we studied the IETS spectra of our BDT molecular junctions with MLG electrodes, which were found to be consistent with previously reported theoretical and experimental results [48, 59–66]. From this, we ascertained that IETS signals can be successfully observed in graphene-interlayer molecular junctions and confirmed the molecular signatures in these junctions. The principles of IETS have previously been explained in the literature [61, 62]. Here, we will briefly reiterate them. When a negative voltage is applied to an Au/MLG electrode, its Fermi level is raised (figure 4(a)). Then, an electron on the Au/MLG electrode begins to tunnel into the empty states of the right-hand Au electrode through an energy-conserving process known as elastic tunneling (black arrow). Alternatively, the electron can also tunnel through the junction with an energy loss by delivering an energy quantum, $\hbar\omega$, into a localized vibrational mode of the molecule. This energy is used to excite the molecule's vibrational mode. The electron is eventually transmitted through the molecule through an inelastic tunneling process (red arrow). The inelastic channel is available only if the bias V_0 exceeds the specific phonon energy $\hbar\omega/e$. When only the elastic tunneling channel is

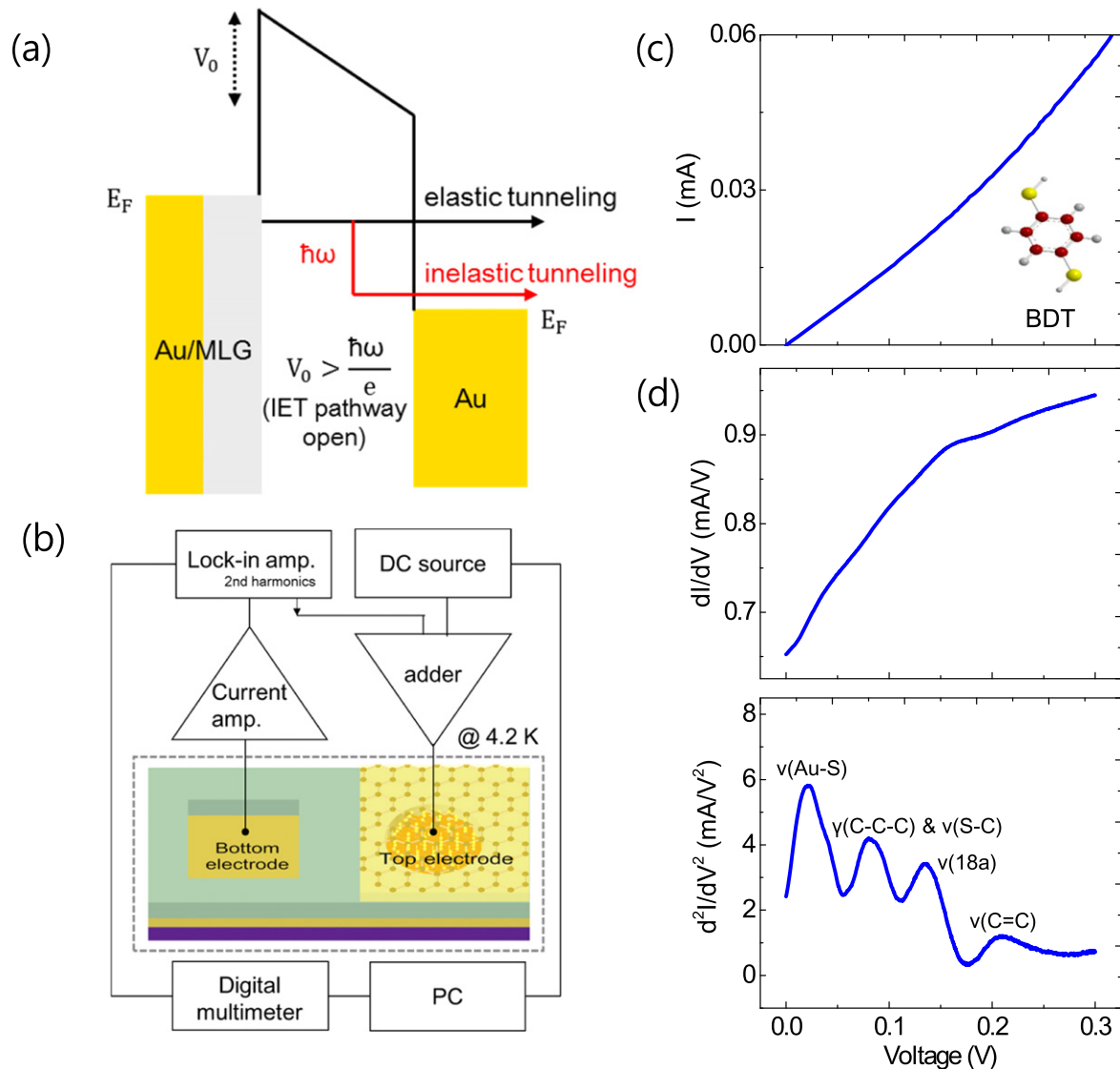


Figure 4. (a) Energy band diagram describing the principles of IETS. The black arrow represents elastic tunneling, and the red arrow represents transmission through the molecule via an inelastic tunneling process. The inelastic channel is available only when the bias voltage V_0 exceeds the specific phonon energy $\hbar\omega/e$. (b) Circuit diagram of our IETS setup. (c) $I(V)$, dI/dV , and d^2I/dV^2 plots of a BDT molecular device with a graphene electrode. In the d^2I/dV^2 plot, IETS peaks can be observed at 21, 82, 136, and 209 mV.

open, the current will increase linearly with an increase in voltage. However, when the inelastic channel becomes available at the threshold voltage ($V_0 = \hbar\omega/e$), this effect creates a small shunt in the slope of the I - V curve. In the conductance ($dI/dV - V$) graph, a step is formed at V_0 . At the same time, a peak appears in the second derivative ($d^2I/dV^2 - V$) graph, namely, an IETS peak. Multiple peaks can be observed if multiple molecular vibrational modes exist; therefore, analyzing the positions of the IETS peaks informs us of the intrinsic vibrational characteristics of the molecule (s) in a junction. Figure 4(b) presents the circuit diagram of our IETS setup. Because the inelastic tunneling current is a very small portion of the overall tunneling current, it is necessary to use an AC modulation technique with LIAs to directly identify the second derivative of the current. We measured the first and second harmonic signals, which are

proportional to dI/dV and d^2I/dV^2 , respectively; then, after adjusting parameters such as the LIA amplitude, LIA sensitivity, current amplifier sensitivity, and transformer factor, we identified the exact dI/dV and d^2I/dV^2 values. Additionally, the IETS measurements were performed at 4.2 K to prevent thermal broadening of the signals. Figure 4(c) shows the $I(V)$, dI/dV , and d^2I/dV^2 plots of our BDT molecular devices with MLG electrodes. The current-voltage measurements were performed from 0 to 0.3 V. The current-voltage (I - V) graph appears as a smooth curve without any kinks. This shape indicates that the contribution from inelastic tunneling is far smaller than the elastic tunneling current, causing the slope shunt in the I - V graph to be barely noticeable. However, the conductance (dI/dV) curve abruptly increases at certain specific voltages. The shape of this graph shows clear evidence of inelastic tunneling. In the d^2I/dV^2 plot, an obvious inelastic tunneling

phenomenon is evident. Several peaks are apparent at 21, 82, 136, and 209 mV, namely, the IETS peaks. The first peak, at 21 mV, is the $\nu(\text{Au-S})$ peak, which corresponds to a strong stretching energy between the thiol end groups and the Au atoms in the bottom electrode [48, 59–66]. The other three peaks originate from the intrinsic vibrational modes of the phenyl ring. The second peak, at 82 mV, is expected to arise from the C–C–C in-plane bending mode $\gamma(\text{C-C-C})$ and the S–C stretching mode $\nu(\text{S-C})$ [48, 59–66]. The third and fourth peaks, at 136 and 209 mV, originate from the $\nu(18a)$ C–H in-plane stretching and $\nu(\text{C=C})$ stretching modes [48, 59–66]. Our experimental results are well consistent with various previous IETS theories and experiments regarding Au–BDT–Au single-molecule junctions [48, 59, 60, 64, 66]. As a result, the role of the BDT molecule as an active transport channel in our molecular device was confirmed by this IETS experiment. One interesting feature is that the intensity of the peaks decreases in the following order: $\nu(\text{Au-S}) > \gamma(\text{C-C-C})$ and $\nu(\text{S-C}) > \nu(18a) > \nu(\text{C=C})$. This means that electron tunneling through the Au–S bond is the most favorable inelastic pathway in this junction. Lin *et al* theoretically suggested that the origin of the intensity ordering of the IETS peaks of an Au–BDT–Au junction is the rotation of the BDT molecule around its S–S axis and that this rotational freedom permits variations in the intensity of each peak [64, 66]. The other noticeable feature is that no clear trace of the graphene electrode is observed in the IETS signals even though MLG exhibits a strong Raman shift peak at approximately 1580 cm^{-1} (196 mV) [67]. Moreover, many other IETS peaks of graphene have also been reported recently [68–71]. However, in this study, we observed only the molecular peaks. This finding implies that the graphene electrode in this metal–molecule–graphene system yields only weak signals and that the weak graphene peaks were overlapped with stronger molecular excitations. However, further theoretical and experimental studies of the electron–phonon interactions in molecular junctions with graphene electrodes will certainly be necessary in the future.

4. Conclusion

In summary, we investigated the electrical characteristics of benzenedithiolate molecular electronic devices with graphene electrodes. The devices were fabricated on both rigid and flexible substrates. We investigated the basic properties of tunneling transport in these devices through current–voltage, molecular-length-dependent, and temperature-dependent characterizations. Additionally, we examined the reliability of the molecular devices fabricated on flexible substrates under various mechanical bending conditions. The electrical characteristics of the devices were well maintained in all tested bending environments. Finally, we observed the IETS peaks of the fabricated graphene–interlayer molecular junctions and demonstrated the role of the benzenedithiolate molecule as an active tunneling component in these molecular junctions. This study extends our understanding of the electrical characteristics of conjugate molecular junctions with graphene

electrodes and may thus contribute to the development of reliable device fabrication platforms and future applications of molecular electronics.

Acknowledgments

The authors appreciate the financial support provided by the National Creative Research Laboratory program (Grant No. 2012026372) through the National Research Foundation of Korea (NRF) funded by the Korean Ministry of Science, ICT & Future Planning. YJ is grateful for the support from the Global PhD Fellowship program (Grant No. 2014H1A2A1021528). G-CY and JY thank the financial support from the Global Research Laboratory Program of the National Research Foundation of Korea (Grant No. NRF-2015K1A1A2033332) and the Research Institute of Advanced Materials (RIAM). HS acknowledges the support by the Basic Science Research Program (NRF-2013R1A1A1076158).

References

- [1] Aviram A and Ratner M A 1974 *Chem. Phys. Lett.* **29** 277
- [2] Reed M A, Zhou C, Muller C J, Burgin T P and Tour J M 1997 *Science* **278** 252
- [3] Chen J, Reed M A, Rawlett A M and Tour J M 1999 *Science* **286** 1550
- [4] Park J *et al* 2002 *Nature* **417** 722
- [5] Nitzan A and Ratner M A 2003 *Science* **300** 1384
- [6] Matsuda K and Irie M 2001 *J. Am. Chem. Soc.* **123** 9896
- [7] Galperin M, Ratner M A, Nitzan A and Troisi A 2008 *Science* **319** 1056
- [8] Love J C, Estroff L A, Kriebel J K, Nuzzo R G and Whitesides G M 2005 *Chem. Rev.* **105** 1103
- [9] Nijhuis C A, Reus W F, Siegel A C and Whitesides G M 2011 *J. Am. Chem. Soc.* **133** 15397
- [10] Behin-Aein B, Datta D, Salahuddin S and Datta S 2010 *Nat. Nanotechnol.* **5** 266
- [11] Zhou C, Muller C J, Deshpande M R, Sleight J W and Reed M A 1995 *Appl. Phys. Lett.* **67** 1160
- [12] Park H, Lim A K L, Alvisatos A P, Park J and McEuen P L 1999 *Appl. Phys. Lett.* **75** 301
- [13] Strachan D R, Smith D E, Johnston D E, Park T H, Therien M J, Bonnell D A and Johnson A T 2005 *Appl. Phys. Lett.* **86** 043109
- [14] Poirier G E 1997 *Chem. Rev.* **97** 4
- [15] Datta S, Tian W, Hong S, Reifenberger R, Henderson J I and Kubiak C P 1997 *Phys. Rev. Lett.* **79** 13
- [16] Simeone F C, Yoon H J, Thuo M M, Barer J R, Smith B and Whitesides G M 2013 *J. Am. Chem. Soc.* **135** 18131
- [17] Nijhuis C A, Reus W F, Barber J R and Whitesides G M 2012 *J. Phys. Chem. C* **116** 14139
- [18] Haick H and Cahen D 2008 *Acc. Chem. Res.* **41** 359
- [19] Kim T-W, Wang G, Lee H and Lee T 2007 *Nanotechnology* **18** 315204
- [20] de Boer B, Frank M M, Chabal Y J, Jiang W R, Garfunkel E and Bao Z 2004 *Langmuir* **20** 1539
- [21] Haick H, Niiitsoo O, Ghabboun J and Cahen D 2007 *J. Phys. Chem. C* **111** 2318
- [22] Walker A V, Tighe T B, Cabarcos O M, Reinard M D, Haynie B C, Uppili S, Winograd N and Allara D L 2004 *J. Am. Chem. Soc.* **126** 3954

- [23] Wang G, Kim T-W, Lee H and Lee T 2007 *Phys. Rev. B* **76** 205320
- [24] Lau C N, Stewart D R, Williams R S and Bockrath M 2004 *Nano Lett.* **4** 4
- [25] Akkerman H B, Blom P W M, de Leeuw D M and de Boer B 2006 *Nature* **441** 69
- [26] Jeong H et al 2014 *Adv. Funct. Mater.* **24** 2472
- [27] Kim D, Jeong H, Lee H, Hwang W T, Wolf J, Scheer E, Huhn T, Jeong H and Lee T 2014 *Adv. Mater.* **26** 3968
- [28] Park S, Wang G, Cho B, Kim Y, Song S, Ji Y, Yoon M-H and Lee T 2012 *Nat. Nanotechnol.* **7** 438
- [29] Wang G, Kim Y, Choe M, Kim T-W and Lee T 2011 *Adv. Mater.* **23** 755
- [30] Li T et al 2012 *Adv. Mater.* **24** 1333
- [31] Seo S, Min M, Lee S M and Lee H 2013 *Nat. Commun.* **4** 1920
- [32] Seo S, Min M, Lee J, Lee T, Choi S-Y and Lee H 2012 *Angew. Chem., Int. Ed. Engl.* **51** 108
- [33] Li T et al 2012 *Adv. Mater.* **24** 1333
- [34] Kim D, Jeong H, Hwang W T, Jang Y, Sysoiev D, Scheer E, Huhn T, Min M, Lee H and Lee T 2015 *Adv. Funct. Mater.* **25** 5918
- [35] Jeong H et al 2015 *Nanotechnology* **26** 025601
- [36] Jeong H et al 2015 *Appl. Phys. Lett.* **106** 063110
- [37] Novoselov K S, Geim A K, Morozot S V, Jiang D, Zhang Y, Dubonos S V, Grigorieva I V and Firsov A A 2004 *Science* **306** 666
- [38] Wang Q H and Hersam M C 2009 *Nat. Chem.* **1** 206
- [39] Kim K S, Zhao Y, Jang H, Lee S Y, Kim J M, Kim K S, Ahn J G, Kim P, Choi J Y and Hong B H 2009 *Nature* **457** 706
- [40] Reina A, Jia X, Ho J, Nezich D, Son H, Bulovic V, Dresselhaus M S and Kong J 2008 *Nano Lett.* **9** 30
- [41] Regan W, Alem N, Aleman B, Geng B, Grit C, Maserati L, Wang F, Crommie M and Zettl A 2010 *Appl. Phys. Lett.* **96** 113102
- [42] Weiss E A, Wasielewski M R and Ratner M A 2005 *Molecular Wires and Electronics* (Berlin: Springer) p 103
- [43] Ng M K and Yu L 2002 *Angew. Chem., Int. Ed. Engl.* **41** 3598
- [44] Collier C P, Wong E W, Belohradsky M, Raymo F M, Stoddart J F, Kuekes P J, Williams R S and Heath J R 1999 *Science* **285** 391
- [45] Tao N J 2006 *Nat. Nanotechnol.* **1** 173
- [46] Choi S H, Kim B and Frisbie C D 2008 *Science* **320** 1482
- [47] Wold D J, Haag R, Rampi M A and Frisbie C D 2002 *J. Phys. Chem. B* **106** 2813
- [48] Song H, Kim Y, Jeong H, Reed M A and Lee T 2011 *J. Appl. Phys.* **109** 102419
- [49] Holmlin R E, Haag R, Chabynyc M L, Ismagilov R F, Cohen A E, Terfort A, Rampi M A and Whitesides G M 2001 *J. Am. Chem. Soc.* **123** 5075
- [50] Jeziorny A 1978 *Polymer* **19** 1142
- [51] Holdsworth P J and Turner-Jones A 1971 *Polymer* **12** 3
- [52] Beebe J M, Kim B, Gadzuk J W, Frisbie C D and Kushmerick J G 2006 *Phys. Rev. Lett.* **97** 026801
- [53] Nie S and Emory S R 1997 *Science* **275** 5303
- [54] Kim Y, Song H, Strigl F, Pernau H F, Lee T and Scheer E 2011 *Phys. Rev. Lett.* **106** 196804
- [55] Reddy P, Jang S Y, Segalman R A and Majumdar A 2007 *Science* **315** 1568
- [56] Jaklevic R C and Lambe J 1966 *Phys. Rev. Lett.* **17** 1139
- [57] Okabayashi N, Konda Y and Komeda T 2008 *Phys. Rev. Lett.* **100** 217801
- [58] Wang W, Lee T, Kretzschmar I and Reed M A 2004 *Nano Lett.* **4** 643
- [59] Kim Y, Pietsch T, Erbe A, Belzig W and Scheer E 2011 *Nano Lett.* **11** 3734
- [60] Song H, Kim Y, Jang Y H, Jeong H, Reed M A and Lee T 2009 *Nature* **462** 1039
- [61] Hansma P K 1977 *Phys. Rep.* **30** 145
- [62] Adkins C J and Phillips W A 1985 *J. Phys. C* **18** 1313
- [63] Taniguchi M, Tsutsui M, Yokota K and Kawai T 2009 *Nanotechnology* **20** 434008
- [64] Lin L L, Wang C K and Luo Y 2011 *ACS Nano* **5** 2257
- [65] Kula M and Luo Y 2008 *J. Chem. Phys.* **128** 064705
- [66] Lin L L, Jiang J and Luo Y 2013 *Physica E* **47** 167
- [67] Ferrari A C et al 2006 *Phys. Rev. Lett.* **97** 187401
- [68] Zhang Y, Brar V W, Wang F, Girit C, Yayon Y, Panlasigui M, Zettl A and Crommie M F 2008 *Nat. Phys.* **4** 627
- [69] Natterer F D, Wyrick J, Chan Y H, Ruan W Y, Chou M Y, Watanabe K, Taniguchi T, Zhitenev N B and Stroschio J A 2015 *Phys. Rev. Lett.* **114** 245502
- [70] Brar V W et al 2010 *Phys. Rev. Lett.* **104** 036805
- [71] Castellanos-Gomez A, Rubio-Bollinger G, Barja S, Garnica M, de Parga A L V, Miranda R and Agrait N 2013 *Appl. Phys. Lett.* **102** 063114